

SPECTRAL ANALOGUES OF BARBARIAN ASTEROIDS AMONG CO AND CV CHONDRITES

PREPRINT

Max Mahlke^{1,2}, Jolantha Eschrig³, Benoit Carry¹, Lydie Bonal³, and Pierre Beck³

¹Université Côte d'Azur, Observatoire de la Côte d'Azur, CNRS, Laboratoire Lagrange, France

²Institut d'Astrophysique Spatiale, Université Paris-Saclay, CNRS, F-91405 Orsay, France

³Université Grenoble Alpes, Institut de Planétologie et d'Astrophysique de Grenoble, CNRS-CNES, 38000 Grenoble, France

ABSTRACT

K- and L-type asteroids are considered to be the parent bodies of CV and CO chondrites. Spectral models of L-types invoke an enrichment in calcium-aluminium-rich inclusions (CAIs) with respect to the chondrites in the meteorite collection. Barbarian asteroids are associated to L-type asteroids yet the relationship between these populations is still not clear. We aim to investigate the link between the K- and L-type and Barbarian asteroids and the CV and CO chondrites by means of spectral matching of a large number of reflectance spectra of objects from either population. We seek to identify matches based on observed rather than modelled spectral features. We employ a matching criterion that accounts for the residuals and the correlation of the spectral features. The only free parameter in the comparison is the degree of alteration of the asteroids with respect to the meteorites expressed via an exponential model. We derive an absolute scale of similarity between the spectra using laboratory data from irradiation experiments. CV_{OxA} chondrites are the best match to the asteroids, in particular to K-type (7 out of 11 asteroids matched) and Barbarians (11 out of 16). CO chondrites provide convincing matches for K-types (5 out of 11) and Barbarians (7 out of 16) as well. A single non-Barbarian L-type is matched to a meteorite. Only a few asteroids are matched to CV_{OxB} and CV_{Red} chondrites. Barbarian asteroids are represented among CO and CV_{OxA} chondrites without requiring an enrichment of CAIs in the asteroids. Four candidate Barbarian asteroids are identified, three of which are classified as K-types. These asteroids are favourable targets for polarimetric observations. The discrepancy between L-type asteroids and CV and CO chondrites is likely related to the ambiguity of the asteroid class itself. An extension of the taxonomy to include polarimetric properties is required.

1 INTRODUCTION

Establishing links between meteorites and their parent asteroids is a fundamental goal of planetary science (Gaffey, 1993; Binzel, 1995; Greenwood et al., 2020; DeMeo et al., 2022). Detailed mineralogical analyses of meteorites allow us to interpret observational features of single asteroids (e. g. McCord et al., 1970; Lazzaro et al., 2000; de León et al., 2004; Dibb et al., 2023) and trends among larger populations (e. g. Fornasier et al., 2010; Thomas & Binzel, 2010; de León et al., 2012; Vernazza et al., 2016; Eschrig et al., 2021, 2022), which in turn are used to infer their dynamical history and to constrain models of the formation of the Solar System.

K- and L-type asteroids are rare both in terms of their absolute number and their mass fraction with respect to the general population of the Main Belt; combined, they represent <10% in a given mass range and section of the Main Belt (DeMeo & Carry, 2013; Mahlke et al., 2022). They are observationally distinct from members of the C- and S-complex due to their moderate albedos and colours, which typically fall between those of these latter complexes (Tedesco et al., 1989; DeMeo & Carry, 2013; Mainzer et al., 2011; Popescu et al., 2018). K-type asteroids show a 1 μm feature associated to forsteritic olivine and, in some cases, a weak 2 μm feature associated to orthopyroxene (Bell, 1988; Mothé-Diniz & Carvano, 2005; Clark et al., 2009). L-type asteroids exhibit a 2 μm feature attributed to Fe²⁺-bearing spinel and a weak or fully absent 1 μm feature attributed to Fe-rich olivine (Burbine et al., 1992; Sunshine et al., 2008). As the depths of both features vary, the spectral appearance of both classes is continuous and members of either class are frequently reclassified into the other one (Bus & Binzel, 2002a; DeMeo et al., 2009; Mahlke et al., 2022).

Based on spectral similarities, K- and L-type asteroids have been associated primarily to two classes of carbonaceous chondrites (CCs), namely CO and CV (Bell, 1988; Burbine et al., 2001; Mothé-Diniz et al., 2008; Clark et al., 2009). These classes of anhydrous CCs show similar and partially overlapping distributions in oxygen-isotope compositions and petrographic properties, including similar volume percentages of chondrules, matrix, and refractory inclusions (Weisberg et al., 2006; Krot et al., 2014). All CO and CV chondrites are of petrographic type 3. They show the largest abundances of refractory inclusions among CCs with 13 vol% and 10 vol% respectively. More specifically, they include calcium-aluminium-rich inclusions (CAIs) and to a lesser degree amoeboid olivine aggregates (AOAs) (<5 vol%, Ebel et al., 2016; Pinto et al., 2021). CAIs are some of the oldest components in chondrites and consist of various minerals including melilite, forsterite and spinel. They are believed to have condensed at high temperatures and low pressures within the solar nebula. AOAs are micro- to millimetre sized aggregates of forsterite, Fe-Ni metal, spinel and anorthite, among others. Most AOAs did not undergo melting (Scott & Krot, 2014).

The key differences between CO and CV chondrites are given in their whole-rock compositions, where the latter are generally enriched in lithophile elements with respect to CO chondrites while CO are generally enriched in siderophile elements. Furthermore, CO chondrites have considerably smaller chondrules (average diameter of 0.15 mm, Krot et al., 2014) compared to CV (1 mm). Spectrally, both chondrite classes show 1 μm features attributed to olivine and 2 μm features attributed to Fe²⁺-bearing spinel (Cloutis et al., 2012b,c). The 2 μm feature is generally absent in CO chondrites of petrographic type ≤ 3.1 , while the 1 μm feature becomes more pronounced with thermal metamorphism

(Cloutis et al., 2012b; Eschrig et al., 2021).

CV chondrites are further subdivided into the reduced CV_{Red} and the oxidised CV_{OxA} and CV_{OxB} (Mcsween, 1977; Weisberg et al., 1997). The subgroups are based on different compositional and petrographic properties (Krot et al., 1995; Cloutis et al., 2012c). In particular, in comparison to CV_{OxA} and CV_{OxB}, CV_{Red} chondrites are characterised by (i) a lower abundance of matrix, (ii) a higher abundance of metal, and (iii) the presence of Ni-poor sulfides. In comparison to CV_{OxB}, CV_{OxA} are characterised by (i) similar matrix abundance, (ii) a higher abundance of metal, (iii) the presence of metal almost exclusively under the form of awaruite, (iv) lower Ni content of sulfides, and (v) lower magnetic susceptibility and saturation remanence (Bonafant et al., 2020). The oxidised CV chondrites (in particular CV_{OxA}) generally have larger petrographic types (>3.6) than the reduced CV and the CO chondrites (Bonafant et al., 2016, 2020). Cloutis et al. (2012c) did not identify differences in the spectral appearance between the three subgroups exceeding the variability of the spectra within a single subgroup, while Eschrig et al. (2021) observe systematic differences in the depths and widths of the 1 μm and 2 μm features, in particular between CV_{Red} and CV_{OxA}. Eschrig et al. (2021) further note the spectral similarity between CO chondrites and the CV_{OxA} subgroup.

While it is commonly assumed that each CC class is derived from an individual parent body, Gattacceca et al. (2020) conclude, based on petrographic and isotopic properties, that oxidised and reduced CV chondrites have two distinct parent bodies. Furthermore, Greenwood et al. (2010) suggest that the oxidised CV subgroups and CK chondrites may have formed in the same parent body given their similar oxygen isotopes and elemental abundances. These authors propose that the thermally metamorphosed CK chondrites represent the core of this parent body while the CV chondrites form the outer shell. A possible remnant of the partially differentiated CV-CK parent body could be the Eos family. Its members are predominantly K-types and show a spectral variability that is consistent with being composed of a partially differentiated ordinary-chondritic parent body (Doressoundiram et al., 1998; Mothé-Diniz et al., 2008; Greenwood et al., 2010). A further candidate family may be the Eunomia family. Its parent body (15) *Eunomia* appears partially differentiated with an olivine-rich composition (Nathues et al., 2005).

Like K-types, L-type asteroids are commonly associated to CO and CV chondrites (Burbine et al., 1992, 2001). Using radiative transfer models, Sunshine et al. (2008) show that the spectra of (234) *Barbara*, (387) *Aquitania*, and (980) *Anacostia* can be modelled using endmembers consisting of olivine, CAI-free matrix from CV_{OxA} Allende, and a subtype of CAI (fluffy type A) common in CV chondrites in addition to a slope component. The derived CAI abundances are between 22 % and 39 %. A large abundance of refractory inclusions would necessitate an early formation of these asteroids, making them the most ancient probes of the Solar System formation among the small bodies (Sunshine et al., 2008).

Devogèle et al. (2018) extend this analysis to a larger sample of L-type asteroids and by including an endmember spectrum consisting of a bulk measurement of CV_{OxA} Y-86751. For the sample of 28 L-types, the required CAI abundance using the same CV_{OxA} Allende endmember as Sunshine et al. (2008) is (28 ± 13) vol%, while for the CV_{OxA} Y-86751 endmember, an

abundance of (14 ± 10) vol% of CAI is required to spectrally match the sample of 28 L-type asteroids. The highest refractory inclusion abundance observed in meteorites is 13 vol% for CO chondrites when accounting for both CAIs and AOA (Brearley et al., 1998; Krot et al., 2014).

A different population of asteroids commonly associated to L-types are the Barbarians. Unlike K- and L-types, this group is defined based on polarimetric rather than spectral features. Specifically, Barbarians are defined based on a high inversion angle ($\alpha_{\text{min}} > 25$ deg) of the negative branch of the polarimetric phase curve, as observed for (234) *Barbara* by Cellino et al. (2006). While Devogèle et al. (2018) concluded that L-types as defined by DeMeo et al. (2009) and Barbarian asteroids are identical populations, Mahlke et al. (2022) show that Barbarians exhibit a spectral variability that is larger than permissible for a single taxonomic class. Nevertheless, Devogèle et al. (2018) show that the Barbarian polarimetric feature is correlated with the modelled abundance of CAI in the asteroid, and the authors suggest CAI enrichment as a possible mechanism for the large polarimetric inversion angle. Frattin et al. (2019) measure $\alpha_{\text{min}} = (22 \pm 1)$ deg for CV_{OxA} Allende and $\alpha_{\text{min}} = (20 \pm 5)$ deg for CV DaG 521 and COs FRO 95002 and FRO 99040, which does not allow the reported correlation to be confirmed or denied. An alternative explanation is a heterogeneity of high- and low-albedo particles on the asteroid surfaces (Gil-Hutton et al., 2008).

In this work, we investigate the spectral match of CO and CV chondrites and K-type, L-type and Barbarian asteroids. One of the main focuses of our analysis is on the question of whether a larger sample size of asteroid, and in particular meteorite spectra, may reveal matches between the chondrites and the asteroids without requiring an enrichment in CAIs. We further divide the CV chondrites into the subgroups CV_{OxA}, CV_{OxB}, and CV_{Red}, in line with the current interpretation of the CV class in the literature. In Sect. 2, we outline the sample preparation of asteroid and meteorite spectra as well as the matching procedure. In Sect. 3, we present our results. In Sect. 4, we draw conclusions based on the derived similarities of the populations.

2 METHODOLOGY

In this section, we first outline our methods of sample collection and preparation, followed by a description of the matching algorithm and the derivation of an absolute similarity scale used to identify matching pairs of asteroids and meteorites.

2.1 Sample selection

2.1.1 Asteroids

The asteroid spectra used here are compiled from various online repositories and publications (refer to Appendix A). The compilation and dataset are described in detail in Mahlke et al. (2022). From this dataset, we select visible-near-infrared (VisNIR) spectra from 0.45 μm to 2.45 μm of asteroids classified as K-types and L-types in Mahlke et al. (2022) (meaning that the probability to be K- or L-type is larger than any other class probability) as well as of confirmed Barbarian asteroids following the census presented in Devogèle et al. (2018). The Barbarian asteroids are not necessarily classified as K- or L-types in Mahlke et al. (2022), as is the case for S-type (980) *Anacostia*. Spec-

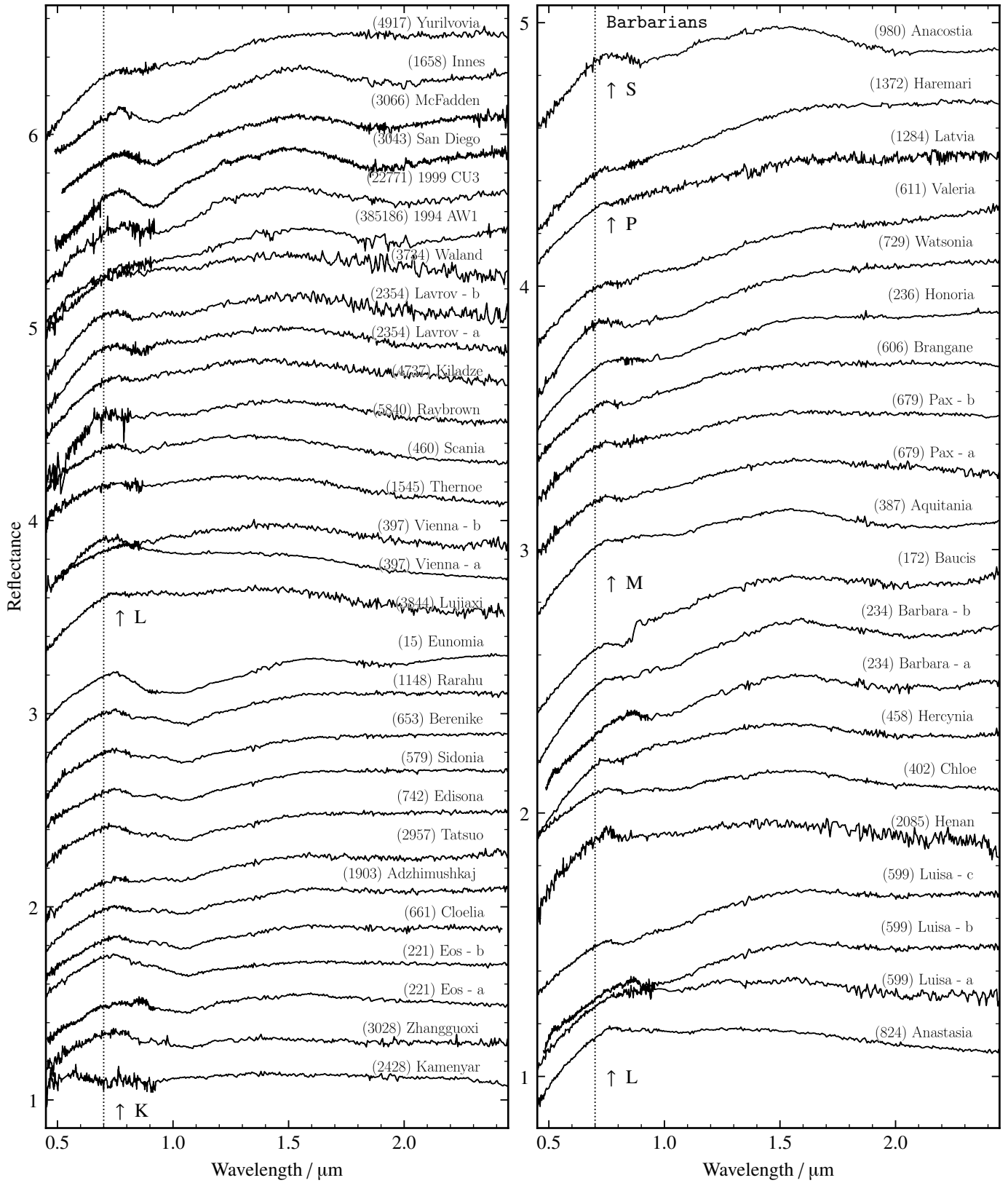


Figure 1: Reflectance spectra of non-Barbarian K- and L-type asteroids (left) and Barbarian asteroids (right). The spectra are sorted by class and decreasing NIR slope. Wavelengths below 0.7 μm (dotted line) are excluded from the following analysis, as outlined in the text. The spectra are shifted along the y-axis for comparability. Their references are given in [Appendix A](#).

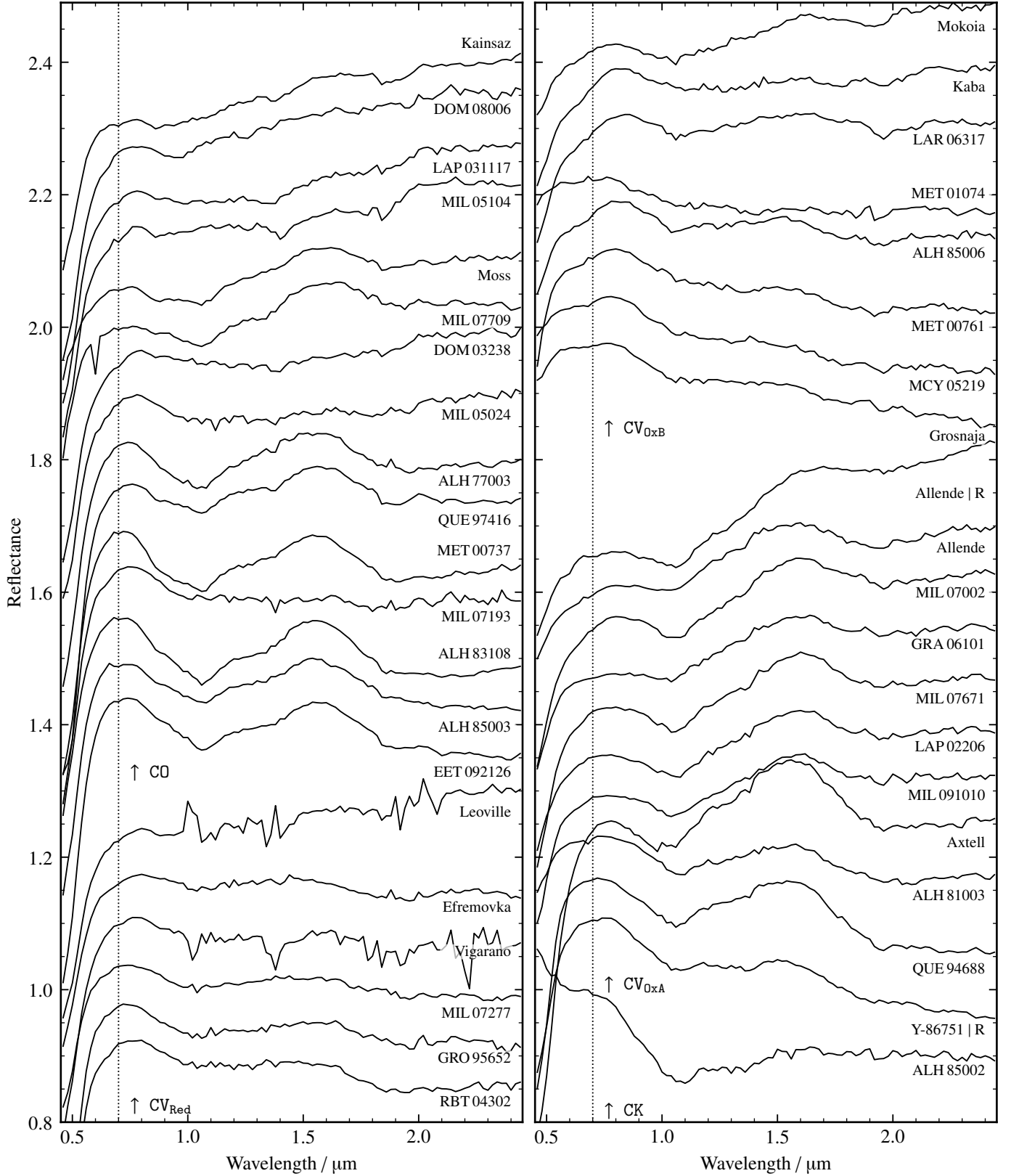


Figure 2: Reflectance spectra of CK, CO, and CV chondrites. The spectra are sorted by class and decreasing NIR slope. The two spectra from the RELAB database are marked by an ‘R’ beside the name of the respective meteorite. Wavelengths below 0.7 μm (dotted line) are excluded from the following analysis. The spectra are shifted along the y-axis for comparability. The spectra of the CO chondrites are from [Eschrig et al. \(2019b\)](#), and those of CV chondrites are from [Eschrig et al. \(2019a\)](#). The measurement of the CK chondrite is unpublished (J. Eschrig).

tra with low signal-to-noise ratio in particular towards the near-infrared (NIR) are rejected following visual inspection. An example is given in Fig. B.1, where the noise towards the NIR does not allow us to reliably identify the presence and depth of a feature around 2 μm . In total, there are 48 spectra, which are shown in Fig. 1. Twelve spectra belong to 11 K-types, 24 spectra to 20 L-types, 9 spectra belong to 8 M-types, 2 spectra belong to 2 P-types, and 1 spectrum belongs to 1 S-type. The 16 Barbarian asteroids include all M-, P-, and S-types, as well as 8 L-type asteroids.

Selecting K- and L-types based on taxonomic classifications is not straightforward because of their spectral variability and the continuity between the classes, making a clear separation challenging (DeMeo et al., 2009; Mahlke et al., 2022). L-types are further prone to misclassification as S-types and vice versa due to their 2 μm bands. Using a probabilistic classification scheme shows the uncertainty in the spectral classification. Table A.1 gives the taxonomic classifications of the asteroids in this study in the systems of Mahlke et al. (2022) and Bus-DeMeo (Bus & Binzel, 2002a; DeMeo et al., 2009). For spectra not classified in DeMeo et al. (2009), we used the `classy` tool¹ to classify them. In some cases, this required extrapolation of the observed spectral range. The maximum extrapolated range represents 7.1% of the classified spectrum and hence we do not expect this to affect the resulting classification.

As class definitions in Mahlke et al. (2022) are based on Gaussian distributions, the large spectral variability among L-types necessarily leads to the inclusion of edge cases with significant probabilities of belonging to other taxonomic classes, as shown in Table A.1. Example objects are (1658) *Innes* and (980) *Anacostia*. The class probabilities could be used to exclude asteroids from this study in case of an ambiguous classification; however, we choose not to cut the sample based on the probabilities as the following analysis is on a per-object basis and there is no downside to having a potentially misclassified object in the comparison sample.

Further indicated in Table A.1 is the Barbarian nature of the asteroids, based on results from Devogèle et al. (2018) and Bendjoya et al. (2022). Asteroids are marked with a dash if there are insufficient polarimetric data to determine the Barbarian nature.

Figure 1 shows the variability in spectral features and slopes of the K- and L-types as well as of the Barbarian asteroids. The 2 μm band in L-types varies between prominent (e. g. (234) *Barbara*) and nearly absent ((824) *Anastasia*), while some depict a 1 μm band ((3043) *San Diego*) and resemble S-types. For K-types, a variability of the strength of the 1 μm band is well established (Clark et al., 2009). Among the Barbarian asteroids, we observe a similar variability to that seen among the L-types. (824) *Anastasia* appears blue and featureless while (980) *Anacostia* has a red slope with bands present around 1 μm and 2 μm . Nevertheless, as discussed in Mahlke et al. (2022), the class boundaries between K, L, and M based on VisNIR spectra and visual albedos are continuous, giving rise to edge cases without a conclusive classification.

Six asteroids are represented with more than one spectrum in the sample. We choose this to understand the systematic uncertainty that enters into the asteroid–meteorite matching when using a single spectrum of an individual as a reference. For ex-

ample, the duplicate spectra *b* and *c* of (599) *Luisa* contain the same NIR spectrum but different visible spectra, which results in a noticeable shift of the visible feature from around 0.8 μm to 1.0 μm .

2.1.2 Meteorites

A total of 41 reflectance spectra of 40 individual chondrites are analysed in this study, including 15 CO and 24 CV spectra, the latter of which are divided into 10 CV_{OxA}, 8 CV_{OxB}, and 6 CV_{Red}, as shown in Fig. 2. The majority of the spectra were presented in Eschrig et al. (2019a,b, 2021) and are available online in the SSHADE database (Schmitt et al., 2018).^{2,3}

We further add one spectrum for each of the CV_{OxA} chondrites Allende and Y-86751 from the RELAB database (Pieters & Hiroi, 2004, respective specimen IDs: MT-TJM-071 and MP-TXH-009). These spectra are used in Sunshine et al. (2008) and Devogèle et al. (2018) to study the mineralogical abundances of L-type asteroids and therefore allow us to compare our results to those studies. We do not add more spectra from RELAB as we aim for consistent sample treatment and measurement conditions for the meteorite spectra in order to reduce the spectral variability introduced by changes in observation geometry and sample properties such as the grain size (Cloutis et al., 2012c,b; Eschrig et al., 2021). Finally, we acquire a spectrum of CK4 chondrite ALH 85002 to extend the sample towards the analogue proposed by Mothé-Diniz et al. (2008) for K-types of the Eos family. More samples of CK chondrites were not available to us for this work. Given the variability of CK chondrites reported by Cloutis et al. (2012a), any conclusion based on a single sample is highly tentative. Nevertheless, we choose to include this sample based on the relationship between CV and CK chondrites proposed by Greenwood et al. (2010).

Apart from the two RELAB measurements, all reflectance spectra were acquired with a consistent sample preparation and measurement procedure. The chondrite samples were hand ground to a powder of approximately submillimetre grain size (Garenne et al., 2016) using a pestle and mortar. In contrast to the method used to obtain the RELAB spectra, no sieving was performed by Eschrig et al. (2021) in order to avoid a selection effect of harder-to-grind chondrite components. Garenne et al. (2016) estimate the average grain size of hand-ground chondrite samples to 100 μm to 200 μm . 50 mg of the chondrite powder was added to a sample holder and the surface was flattened using a spatula to facilitate comparison between measurements. Reflectance spectra in the range of 340 nm to 4200 nm were obtained at 80 °C under vacuum to eliminate terrestrial water contamination using a measuring geometry of $i = 0^\circ$, $e = 30^\circ$.

There are two spectra available for CV Allende, one from RELAB and one from Eschrig et al. (2021). While the former was measured on a CAI-free powder of <38 μm grain size under ambient temperatures and pressures, the spectrum in Eschrig et al. (2021) was taken on the bulk powder using the conditions described above. These differences in measuring conditions may partly explain the differences observed between these two spectra. Both the removal of the CAI component and the decrease

¹<https://classy.readthedocs.io>

²https://www.sshade.eu/data/experiment/EXPERIMENT_LB_20191220_001

³https://www.sshade.eu/data/experiment/EXPERIMENT_LB_20191220_002

in grain size of the RELAB sample with respect to that from [Eschrig et al. \(2021\)](#) could explain the decrease in band depth of the $2\ \mu\text{m}$ feature ([Mustard & Hays, 1997](#); [Eschrig et al., 2022](#)).

[Fig. 2](#) reveals a large degree of spectral variability between the meteorite classes and even among samples of the same class or subclass. Both CV and CO spectra are variable in band structure and slope. The spectra of CO chondrites tend to have more pronounced $1\ \mu\text{m}$ bands though there are samples such as MIL 07193, which show no band at all. [Cloutis et al. \(2012c\)](#) note that the petrologic parameters used to differentiate CO and CV chondrites do not give rise to appreciable differences in the spectra, in particular on fine-grained parent body surfaces. Furthermore, the authors cannot establish spectral differences between CV subtypes, while they are apparent in the sample of [Eschrig et al. \(2021\)](#), as shown in [Fig. 2](#) and discussed in the original publication. The spectra of CV_{OxA} look similar to those of CO chondrites. Also apparent are large differences in the visible slope, likely due to the formation of ferric oxides as part of terrestrial weathering ([Salisbury & Hunt, 1974](#); [Gooding, 1982](#); [Cloutis et al., 2012c](#); [Eschrig et al., 2021](#)), and we exclude the region below $0.7\ \mu\text{m}$ from the analysis due to this systematic uncertainty.

2.2 Spectral matching of asteroids and meteorites

We first define a criterion to quantify the similarity between two reflectance spectra and then outline the assumptions we make to define an absolute scale of similarity.

2.2.1 Similarity criterion Φ

To quantify the similarity between two reflectance spectra \mathbf{X} and \mathbf{Y} consisting of N datapoints x_i and y_i with $i \in \{1, \dots, N\}$ sampled at the same wavelengths λ_i , we combine two criteria presented in [Popescu et al. \(2012\)](#). The first criterion quantifies the similarity by means of the residuals e_i given by $(x_i - y_i)$,

$$\Phi_{\text{res}} = \frac{1}{N} \sqrt{\sum_i^N (e_i - \bar{e})^2}, \quad (1)$$

where \bar{e} is the mean residual value. Smaller values of Φ_{res} indicate an increasing similarity between the spectra. The second criterion quantifies the covariance $\text{cov}(\mathbf{X}, \mathbf{Y})$ of the curves,

$$\Phi_{\text{cov}} = \frac{\text{cov}(\mathbf{X}, \mathbf{Y})}{\sigma_{\mathbf{X}}\sigma_{\mathbf{Y}}}, \quad (2)$$

where $\sigma_{\mathbf{X}}$ and $\sigma_{\mathbf{Y}}$ are the respective standard deviations. Larger values of Φ_{cov} indicate an increasing similarity between the spectra. In particular, the correlation of the spectra quantifies their similarity in potential absorption features. Both criteria are combined to give the similarity criterion Φ ,

$$\Phi = \frac{\Phi_{\text{cov}}}{\Phi_{\text{res}}}, \quad (3)$$

where larger values indicate an increasing similarity between the spectra.

Prior to the comparison, all reflectance spectra are smoothed using a Savitzky-Golay filter ([Savitzky & Golay, 1964](#)). This filter computes a polynomial fit to all data points in a rolling window

of a user-defined width and replaces the value at the centre of the window by the value of the fitted polynomial. By visual inspection of the smoothing, we choose a polynomial degree of 3 and a rolling-window width of 41 data points. For (172) *Baucis*, we use a width of 95 data points to smooth the systematic artefact around $0.8\ \mu\text{m}$. Finally, the spectra are resampled to a uniform wavelength grid to ensure that the computed similarity criteria are comparable.

2.2.2 Accounting for secondary spectral alterations

The reflectance spectra of asteroids and meteorites are shaped primarily by their chemical composition and mineralogy, which are the properties we aim to compare in asteroids and meteorites. However, in second order, spectra are shaped by surface properties such as the regolith grain size and porosity as well as alterations due to the space- or the terrestrial environment ([Reddy et al., 2015](#); [Cloutis et al., 2018](#); [Eschrig et al., 2022](#)). These secondary effects generally lead to a difference in the spectral appearance of meteorites and their parent-body asteroid populations, which has to be accounted for when establishing compositional connections ([Gaffey, 1993](#); [Binzel, 1995](#); [DeMeo et al., 2022](#)). In particular, for carbonaceous chondrites, observing geometry and surface properties such as grain size lead to considerable changes in the spectral appearance, that is, larger than differences due to space weathering ([Cloutis et al., 2012b,c](#); [Brunetto et al., 2014](#); [Lantz et al., 2015, 2017](#); [Ver-nazza et al., 2016](#)). However, these effects generally alter the spectral slope and the depth of absorption bands rather than the central wavelength ([Brunetto et al., 2014](#); [Cloutis et al., 2012c](#); [Beck et al., 2021](#)). In this work, we therefore make the assumption that the secondary changes of the spectral continuum may be described in a joint model, for which we use the exponential space-weathering model derived in [Brunetto et al. \(2006\)](#):

$$W(\lambda) = K \exp\left(-\frac{C_S}{\lambda}\right), \quad (4)$$

where W is the weathering function given by the ratio of the meteorite to the asteroid spectrum, K a normalising scale factor, and C_S the strength parameter of the space weathering. In the following, we refer to this model as the alteration model in order to highlight the fact that we account for all secondary spectral alterations with this exponential function, including but not limited to the space weathering. The larger C_S , the stronger the exponential alteration of the asteroid spectrum with respect to the meteorite spectrum. Negative values of C_S correspond to an asteroid spectrum that is redder than the meteorite spectrum, and positive C_S corresponds to a blueing of the asteroid. As mentioned above, we limit the spectral comparison to the range of $0.7\ \mu\text{m} \leq \lambda \leq 2.45\ \mu\text{m}$.

We therefore identify potential matches between asteroids and meteorites by evaluating the similarity of their ratio to the alteration model given in [Eq. \(4\)](#) using the similarity criterion Φ given in [Eq. \(3\)](#). As we do not know the absolute values of the asteroid reflectance spectra, we normalise the ratio to a unit \mathbb{L}_2 norm prior to fitting the exponential model.

2.2.3 Quantification of similarity

[Brunetto et al. \(2006\)](#) derive the model in [Eq. \(4\)](#) under the assumption that space weathering only marginally affects absorp-

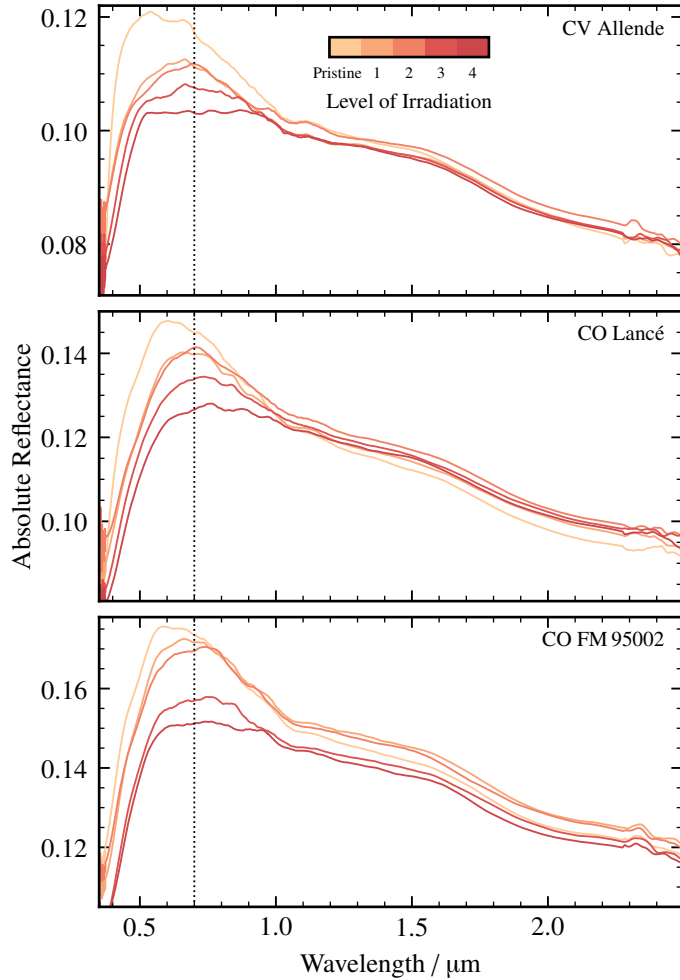


Figure 3: Reflectance spectra of pristine and irradiated carbonaceous chondrites from Lantz et al. (2017). Wavelengths below the dotted vertical line at $0.7\ \mu\text{m}$ are not accounted for in the analysis due to terrestrial weathering. Data courtesy of C. Lantz.

tion features. This assumption is validated for ordinary chondritic samples and mafic silicates. We therefore have to examine whether the model holds for CV/CO-like material as well. Furthermore, to assess the similarity of a match, we require a scale that indicates whether the computed values of Φ are in agreement with the assumption that differences are induced by secondary alterations rather than by mineralogical or compositional features. We validate the model approach and compute this scale using results from irradiation experiments presented by Lantz et al. (2017) who irradiated spectra of CV3 Allende and CO3 chondrites Lancé and FM95002 with He^+ ions. The VisNIR spectra of the pristine and irradiated sample are shown in Fig. 3. For each level of irradiation, we divide the irradiated spectra of each meteorite by their pristine spectrum and compute the Φ criterion between the obtained ratio and the fitted alteration model. Two example fits are shown on the left-hand side of Fig. 4 for meteorites Allende and Lancé, showing the highest and the lowest similarity respectively. The right-hand side of Fig. 4 shows the results for all the meteorites at the different irradiation levels. The similarity Φ between ratio and model decreases with increasing degree of irradiation (i. e. increasing

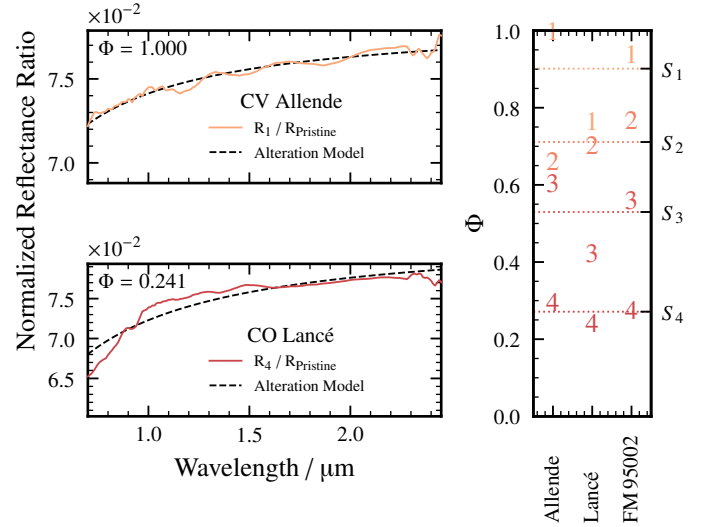


Figure 4: Evaluation of the exponential alteration model using irradiated meteorite samples. Left: Ratios of irradiated to pristine spectra. Here, we show the most (top) and the least (bottom) similar to the fitted alteration model, as quantified by the similarity criterion Φ . Right: Distribution of Φ values for all three reference meteorites and the different irradiation levels j . The dotted horizontal lines indicate the mean similarity S_j for each j .

degree of space weathering) for all three meteorites. We compute the mean Φ for each irradiation level among the three meteorites, indicated by the dotted horizontal lines, and define them as S_j , where $j \in \{1, 2, 3, 4\}$. In Fig. 4 and from here on, we normalise all Φ values by the maximum value from this comparison ($\Phi_{1/\text{Pristine}}$ of CV Allende, top left in Fig. 4) for convenience.

The model in Eq. (4) is used to account for additional spectral alterations. On the other hand, the similarity scale derived in this manner only accounts for changes due to space weathering. As such, it is a strict scale and asteroid–meteorite pairs ruled out in this work may be considered matches if additional discrepancies due to other spectral effects are accounted for. Thus, the strict scale gives an increased reliability for the matches we identify.

3 RESULTS

Each of the 48 asteroid spectra in Fig. 1 is divided by each of the 41 meteorite spectra in Fig. 2 and the resulting ratio is fit by the alteration model in Eq. (4). The similarities Φ of all model fits are shown in Fig. 5. Meteorites are aligned along the y -axis, asteroids along the x -axis. Asteroids are indicated by their number, which is given in green if the asteroid is a confirmed Barbarian and in black otherwise. Darker colours in the figure indicate larger values of Φ and therefore a better description of the asteroid–meteorite ratio by the alteration model. The cells are coloured red (blue) if the asteroid is redder (bluer) than the meteorite. Asteroid–meteorite pairs with Φ values above a value S_j as defined in Sect. 2.2.3 have the respective index j superimposed in black. For these pairs, the spectral differences are well explained by the alteration model and we consider them to be matches. No match reaches the similarity levels S_1 and S_2 . A

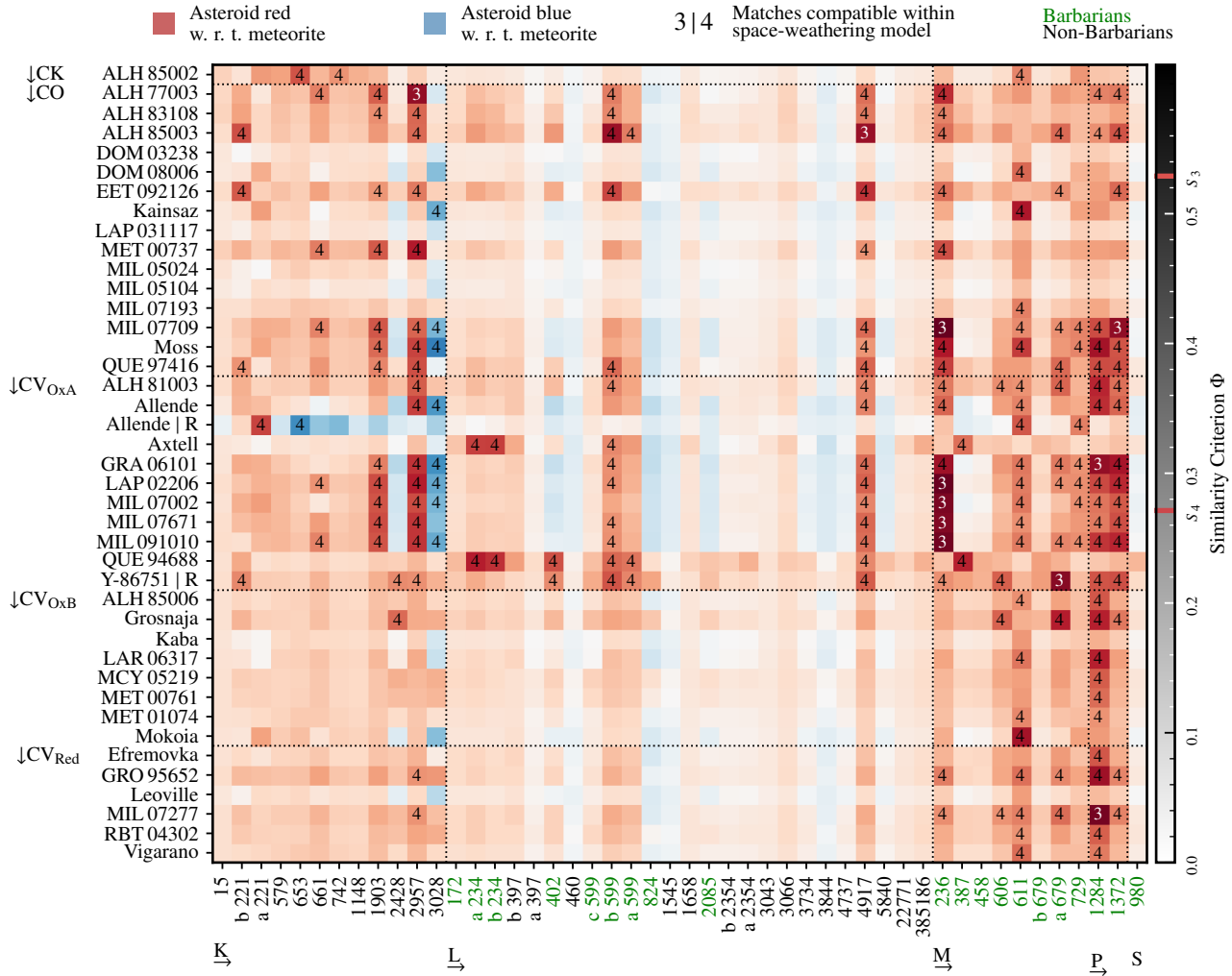


Figure 5: Similarity Φ values of the alteration model to the ratio of the respective pairs of asteroid–meteorite reflectance spectra. Darker colours indicate greater similarity. Red colours show that the asteroid is reddened with respect to the meteorite, and blue colours indicate bluing. Pairs that exceed the similarity levels S_j have the respective j superimposed. Black dotted lines separate different classes of asteroids and meteorites. Asteroids are labelled by their number, while Barbarian asteroids are marked with green labels.

selection of the matches with the largest Φ is shown in Fig. 6, where the asteroid spectra have been divided by the alteration model fit of the asteroid–meteorite ratio. The spectra are normalised to minimise the root-mean-square difference between them.

Fig. 5 shows that CV_{OxA} chondrites have the most matches with asteroids that surpass the S_4 threshold, in particular with K-types (7 out of 11 asteroids) and Barbarians (12 out of 16). For non-Barbarian L-types, only (4917) *Yurilvovia* is a match, for 9 out of 11 chondrites. The remaining matches for CV_{OxA} chondrites are almost exclusively for confirmed Barbarians. Only half of the L-type Barbarians are matched to chondrites, and all the matches are to different CV_{OxA} chondrites than for the non-L-type Barbarians. (234) *Barbara* matches Allende and QUE 94688; the latter match is shown in the bottom-right panel of Fig. 6. (402) *Chloe* and (599) *Luisa* match QUE 94688 as well, while non-L-type Barbarians do not show similarities to this specific CV_{OxA} chondrite, with the exception of (387) *Aquitania*. Axtell is fur-

ther only matched by (387) *Aquitania* and no other non-L-type Barbarian. However, this latter group of asteroids shows large similarities to the remaining CV_{OxA} chondrites, with the exception of (458) *Hercynia* and one spectrum of (679) *Pax*. (980) *Anacostia* does not resemble any meteorite in this study, which is consistent with its classification as S-type in Mahlke et al. (2022). Among K-types, (1903) *Adzhimushkaj* and (2957) *Tat-suo* match 5 and 8 of the 11 CV_{OxA} meteorites, respectively. (3028) *Zhangguoxi* matches 5 CV_{OxA} chondrites while consistently showing a bluer spectrum than all of them.

Non-L-type Barbarians further match CV_{OxB} and CV_{Red} chondrites (five out of nine), while L- and K-types do not, with two exceptions among K-types. We note that if an asteroid matches a CV_{OxA} chondrite, it tends to match a CO chondrite as well.

CO chondrites show a dichotomy, 6 out of 15 have noticeably smaller mean Φ scores than the others in Fig. 5. Five out of 11 K-types and 7 out of 16 Barbarians are matched to CO chondrites.

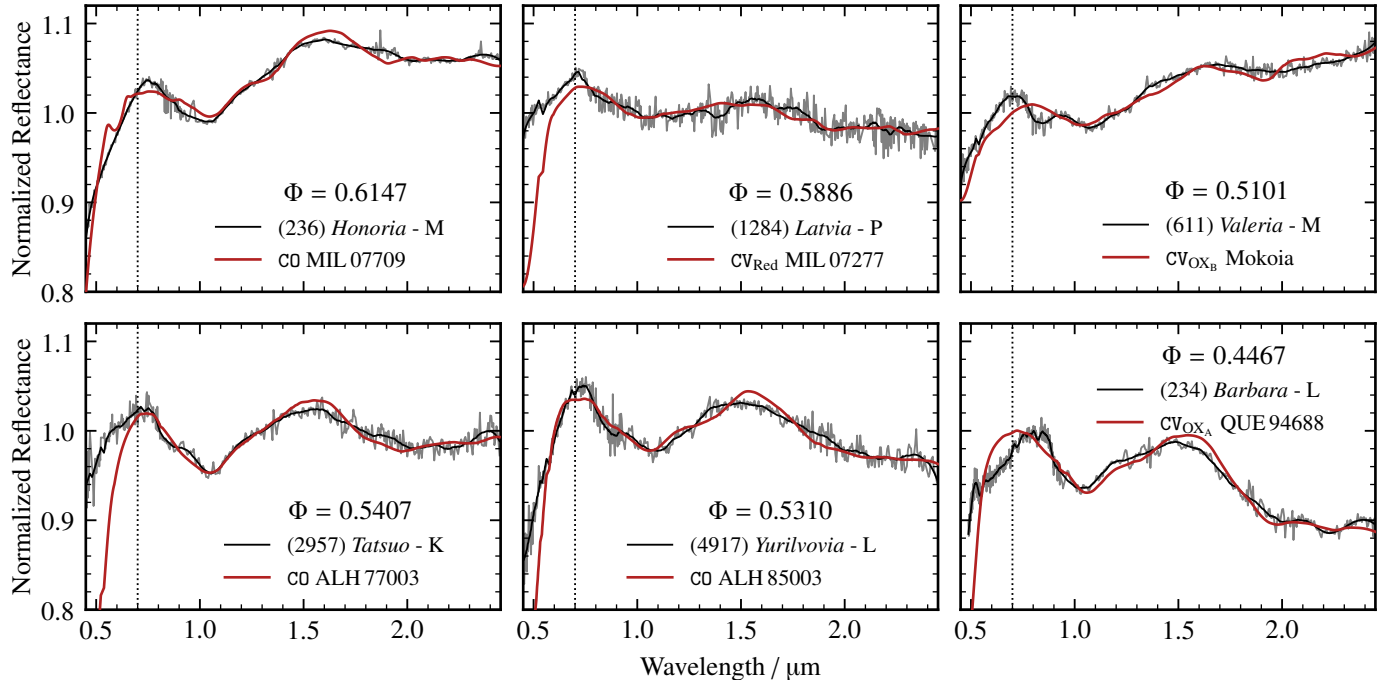


Figure 6: Example matches of asteroids and meteorites. The asteroid spectra (black, solid) have been divided by the exponential alteration-model fitted to the ratio of the asteroid and meteorite spectrum. The similarity Φ between the asteroid spectra and the meteorite spectra (red) does not account for wavelengths below $0.7 \mu\text{m}$ (vertical, dotted line). The light grey and thick black lines show the spectra before and after smoothing, respectively. The given asteroid classes are from [Mahlke et al. \(2022\)](#). The spectrum of (234) *Barbara* is the one from [DeMeo et al. \(2009\)](#).

For non-Barbarian asteroids, only (4917) *Yurilvovia* matches CO chondrites, most consistently with ALH 85003.

The CK chondrite ALH 85002 shows the greatest similarity to K-types and matches (653) *Berenike* and (742) *Edisona*. On the other hand, (980) *Anacostia* is among the least similar asteroids to the ensemble of meteorites and does not have any match, which is likely due to its pronounced $1 \mu\text{m}$ band.

4 DISCUSSION

Under the model assumptions outlined in [Sect. 2](#), we draw the following conclusions from the spectral comparison.

4.1 Matches among CO and CV for Barbarians

We identify several CO and CV chondrites that match Barbarian asteroids, including (234) *Barbara*, which shows a prominent $2 \mu\text{m}$ band and is matched to CV_{oxA} chondrites Axtell and QUE 94688. The latter match is shown in [Fig. 6](#). (387) *Aquitania* is matched to the same meteorites, while (599) *Luisa* matches a variety of CV_{oxA} and CO chondrites. These asteroids were subjects of the studies of [Sunshine et al. \(2008\)](#) and [Devogèle et al. \(2018\)](#) and were shown to match the CV endmember spectra after adding CAI components to the radiative transfer models. The two meteorite spectra used in these latter works (marked with the suffix ‘R’ in [Fig. 5](#)) do not match (234) *Barbara* or (387) *Aquitania* in this study either, which are the two Barbarians with the most prominent $2 \mu\text{m}$ bands. However, (599) *Luisa* is considered a match to CV_{oxA} Y-86751. Overall, non-L-type Barbarians (generally showing weaker $2 \mu\text{m}$ bands than their L-type

counterparts) are more similar to the meteorite spectra. CV_{oxA} chondrites are the most similar to Barbarian asteroids, while CO chondrites further show considerable similarities to Barbarians as well. The fact that the matched L-type Barbarians are associated to different CV_{oxA} than the non-L-type Barbarians highlights the spectral variability in terms of the Barbarian features. This finding further strengthens the link to CV_{oxA} chondrites, as the groups display a similar feature variability.

Barbarians (824) *Anastasia* and (980) *Anacostia* are not represented among the CO and CV chondrites. Both asteroids represent the spectral extremes of the Barbarian variability, both in terms of features (feature-poor versus feature-rich) and NIR slopes (blue versus red). A possible explanation is therefore that the corresponding extreme endmembers of the chondrites are not present in this study. Furthermore, (172) *Baucis* has no match.

4.2 Possible Barbarians

Based on the spectral similarities between CV_{oxA} chondrites and Barbarian asteroids, it may be worthwhile investigating the Barbarian nature of the remaining four asteroids that show significant similarities to the chondrites, which are the K-types (1903) *Adzhimushkaj*, (2957) *Tatsuo*, (3028) *Zhanguoxi*, and L-type (4917) *Yurilvovia*. To our knowledge, no polarimetric phase curves have been observed for these targets. We recommend prioritising them in order to confirm or rule out their Barbarian nature.

4.3 Matches with K-type asteroids inconclusive

Apart from three asteroids ((1903) *Adzhimushkaj*, (2957) *Tat-suo*, and (3028) *Zhangguoxi*, refer to next part), K-types only match a few meteorites in this study, mostly CO and CV_{OxA} chondrites. (653) *Berenike* and (742) *Edisona* match the only CK chondrite ALH 85002. Both are members of the Eos-family, for which [Mothé-Diniz et al. \(2008\)](#) suggested CK chondrites as analogue materials based on comparison of NIR spectra. A larger comparison of K-types and CK chondrites using a consistent meteorite dataset could strengthen this link.

Considering the relationship between CV and CK chondrites proposed by [Greenwood et al. \(2010\)](#), we observe that two out of three matches with CK ALH 85002 are also matches to CV_{OxA} chondrites. However, as noted above, our small sample size prevents us from reaching any form of conclusion here.

4.4 Non-barbarian L-types are not parent bodies of CO and CV

The majority of non-Barbarian L-types are neither matched by CO nor CV. Even not considering possible class interlopers like (1658) *Innes*, (3043) *San Diego*, or (3066) *McFadden* (all three with considerable probability of being S-types), L-types show little similarity to the chondrites in this study. Based on the comparison here, these L-types may be ruled out as parent bodies of CO and CV chondrites.

4.5 Asteroid taxonomy would benefit from polarimetric measurements

The results displayed in [Fig. 5](#) clearly show that Barbarian asteroids should have their own taxonomic class. However, their spectral variability prevents this in a taxonomic scheme based on spectroscopy and albedo only. Polarimetric properties should therefore be added to the asteroid taxonomy. [Mahlke et al. \(2022\)](#) highlight that polarimetric measurements are the most promising observable to resolve compositional ambiguities in the M-complex. The C-complex may further benefit significantly from the addition of polarimetric measurements into the taxonomic scheme including VisNIR spectra and the visual albedo.

The addition of polarimetric properties to the taxonomy is currently challenging because of the low numbers of observed asteroids. Efforts such as the Calern Asteroid Polarization Survey (CAPS, [Bendjoya et al., 2022](#)) are valuable steps towards a more descriptive taxonomy.

4.6 Spectral matching for CCs requires larger sample size

In [Sect. 2](#), we highlight the variability of reflectance spectra of both asteroids and meteorites. The analysis in [Sect. 3](#) shows that this variability can alter the interpretation significantly: for any asteroid and meteorite population combination (except for L-types and CV_{OxB} and CV_{Red}), we identify both matching and non-matching pairs. Relations between populations may therefore only be established reliably when regarding a large number of objects. The three spectra of (599) *Luisa* illustrate this issue: based on spectrum (a), (599) *Luisa* does not match any meteorite in the comparison, while the spectra (b) and (c) are matched to 13 and 3 meteorites, respectively.

Concerning the spectra of meteorites, the variability based on the

sample processing and observation technique used is well established. Here, we note in particular that the spectra of Allende from [Eschrig et al. \(2019a\)](#) and from the RELAB database are matched to different asteroids, in agreement with the different sampling procedures outlined in [Sect. 2](#).

5 CONCLUSION

K- and L-type asteroids are rare and have been associated to various classes of CC. For L-type asteroids, an enrichment in refractory inclusions is considered necessary to arrive at satisfying matches with meteorite spectra. In this study, we perform a large-scale comparison of asteroids and meteorites, focusing on K- and L-types as well as Barbarian asteroids and on their proposed matches, the CO and CV chondrites. The employed matching criterion Φ emphasises the correlation between the compared reflectance spectra, which translates into an emphasis on matching absorption features. Spectral alterations are accounted for in a single exponential model function. We establish matches between Barbarian asteroids and CO and CV chondrites that do not require any additional spectral component. Four candidate Barbarian asteroids are identified based on their matches to the same chondrite classes as established Barbarians. For K-types and L-types, matches among CO and CV chondrites are sparse, and we rule out the possibility that these chondrite classes originate from non-Barbarian L-type asteroids.

ACKNOWLEDGEMENTS

The authors thank the referee Julia de León for the thorough and constructive review which improved the manuscript. The authors further thank Celine Lantz for providing the data of the irradiation experiments.

MM acknowledges funding from the European Space Agency in the framework of the Network Partnering Initiative. The view expressed in this publication can in no way be taken to reflect the official opinion of the European Space Agency.

Parts of this work have been funded by the ERC grant SOLARYS ERC-CoG2017-771691.

All (or part) of the data utilised in this publication were obtained and made available by the MITHNEOS MIT-Hawaii Near-Earth Object Spectroscopic Survey. The IRTF is operated by the University of Hawaii under contract 80HQTR19D0030 with the National Aeronautics and Space Administration. The MIT component of this work is supported by NASA grant 80NSSC18K0849.

REFERENCES

- Beck, P., Schmitt, B., Potin, S., Pommerol, A., & Brissaud, O. 2021, *Icarus*, **354**, 114066
- Bell, J. F. 1988, *Meteoritics*, **23**, 256
- Bendjoya, P., Cellino, A., Rivet, J.-P., et al. 2022, *A&A*, **665**, A66
- Binzel, R. P. 1995, *Meteoritics*, **30**, 486
- Binzel, R. P. 2001, *Icarus*, **151**, 139
- Binzel, R. P., DeMeo, F., Turtelboom, E., et al. 2019, *Icarus*, **324**, 41

- Bonal, L., Gattacceca, J., Garenne, A., et al. 2020, *Geochim. Cosmochim. Acta*, **276**, 363
- Bonal, L., Quirico, E., Flandinet, L., & Montagnac, G. 2016, *Geochim. Cosmochim. Acta*, **189**, 312
- Brearley, A. J., Jones, R. H., & Papike, J. J. 1998, *Reviews in Mineralogy*, Vol. 36, Chondritic meteorites, C1
- Brunetto, R., Lantz, C., Ledu, D., et al. 2014, *Icarus*, **237**, 278
- Brunetto, R., Vernazza, P., Marchi, S., et al. 2006, *Icarus*, **184**, 327
- Burbine, T. H., Binzel, R. P., Bus, S. J., & Clark, B. E. 2001, *M&PS*, **36**, 245
- Burbine, T. H., Gaffey, M. J., & Bell, J. F. 1992, *Meteoritics*, **27**, 424
- Bus, S. J. & Binzel, R. P. 2002a, *Icarus*, **158**, 146
- Bus, S. J. & Binzel, R. P. 2002b, *Icarus*, **158**, 106
- Cellino, A., Belskaya, I., Bendjoya, P., et al. 2006, *Icarus*, **180**, 565
- Clark, B. E., Ockert-Bell, M. E., Cloutis, E. A., et al. 2009, *Icarus*, **202**, 119
- Cloutis, E. A., Hudon, P., Hiroi, T., & Gaffey, M. J. 2012a, *Icarus*, **221**, 911
- Cloutis, E. A., Hudon, P., Hiroi, T., Gaffey, M. J., & Mann, P. 2012b, *Icarus*, **220**, 466
- Cloutis, E. A., Hudon, P., Hiroi, T., et al. 2012c, *Icarus*, **221**, 328
- Cloutis, E. A., Izawa, M. R., & Beck, P. 2018, *Reflectance Spectroscopy of Chondrites* (Elsevier), 273–343
- de León, J., Duffard, R., Licandro, J., & Lazzaro, D. 2004, *A&A*, **422**, L59
- de León, J., Pinilla-Alonso, N., Campins, H., Licandro, J., & Marzo, G. 2012, *Icarus*, **218**, 196
- DeMeo, F. E., Binzel, R. P., Slivan, S. M., & Bus, S. J. 2009, *Icarus*, **202**, 160
- DeMeo, F. E., Burt, B. J., Marsset, M., et al. 2022, *Icarus*, **380**, 114971
- DeMeo, F. E. & Carry, B. 2013, *Icarus*, **226**, 723
- Devogèle, M., Tanga, P., Cellino, A., et al. 2018, *Icarus*, **304**, 31
- Dibb, S. D., Bell, J. F., Elkins-Tanton, L. T., & Williams, D. A. 2023, *Earth and Space Science*, **10**
- Doressoundiram, A., Barucci, M., Fulchignoni, M., & Florczak, M. 1998, *Icarus*, **131**, 15
- Ebel, D. S., Brunner, C., Konrad, K., et al. 2016, *Geochim. Cosmochim. Acta*, **172**, 322
- Eschrig, J., Bonal, L., & Beck, P. 2019a, NIR reflectance spectrum ($i=0^\circ$, $e=30^\circ$) of bulk CV chondrites under vacuum at $T = 80^\circ\text{C}$, SSHADE/GhoSST (OSUG Data Center). Dataset/Spectral Data
- Eschrig, J., Bonal, L., Beck, P., & Prestgard, T. 2019b, NIR reflectance spectrum ($i=0^\circ$, $e=30^\circ$) of bulk CO chondrites under vacuum at $T = 80^\circ\text{C}$, SSHADE/GhoSST (OSUG Data Center). Dataset/Spectral Data
- Eschrig, J., Bonal, L., Beck, P., & Prestgard, T. 2021, *Icarus*, **354**, 114034
- Eschrig, J., Bonal, L., Mahlke, M., et al. 2022, *Icarus*, **381**, 115012
- Fieber-Beyer, S. K., Gaffey, M. J., Kelley, M. S., et al. 2011, *Icarus*, **213**, 524
- Fornasier, S., Clark, B., Dotto, E., et al. 2010, *Icarus*, **210**, 655
- Frattin, E., Muñoz, O., Moreno, F., et al. 2019, *MNRAS*, **484**, 2198
- Gaffey, M. J. 1993, *Science*, **260**, 167
- Garenne, A., Beck, P., Montes-Hernandez, G., et al. 2016, *Icarus*, **264**, 172
- Gattacceca, J., Bonal, L., Sonzogni, C., & Longerey, J. 2020, *Earth and Planetary Science Letters*, **547**, 116467
- Gietzen, K. M., Lacy, C. H. S., Ostrowski, D. R., & Sears, D. W. G. 2012, *Meteoritics & Planetary Science*, **47**, 1789
- Gil-Hutton, R., Mesa, V., Cellino, A., et al. 2008, *A&A*, **482**, 309
- Gooding, J. L. 1982, *Lunar and Planetary Science Conference Proceedings*, 12, 1105
- Greenwood, R., Franchi, I., Kearsley, A., & Alard, O. 2010, *Geochim. Cosmochim. Acta*, **74**, 1684
- Greenwood, R. C., Burbine, T. H., & Franchi, I. A. 2020, *Geochim. Cosmochim. Acta*, **277**, 377
- Krot, A. N., Keil, K., Scott, E. R. D., Goodrich, C. A., & Weisberg, M. K. 2014, in *Meteorites and Cosmochemical Processes*, Vol. 1, 1–63
- Krot, A. N., Scott, E. R. D., & Zolensky, M. E. 1995, *Meteoritics*, **30**, 748
- Lantz, C., Brunetto, R., Barucci, M. A., et al. 2015, *A&A*, **577**, A41
- Lantz, C., Brunetto, R., Barucci, M. A., et al. 2017, *Icarus*, **285**, 43
- Lazzaro, D., Angeli, C. A., Carvano, J. M., et al. 2007, *NASA Planetary Data System*, EAR–A–I0052–8–S3OS2–V1.0
- Lazzaro, D., Michtchenko, T., Carvano, J. M., et al. 2000, *Science*, **288**, 2033
- Lucas, M. P., Emery, J. P., Hiroi, T., & McSween, H. Y. 2019, *Meteoritics & Planetary Science*, **54**, 157
- Mahlke, M., Carry, B., & Mattei, P.-A. 2022, *A&A*, **665**, A26
- Mainzer, A., Grav, T., Masiero, J., et al. 2011, *ApJ*, **741**, 90
- McCord, T. B., Adams, J. B., & Johnson, T. V. 1970, *Science*, **168**, 1445
- McSween, H. Y. 1977, *Geochim. Cosmochim. Acta*, **41**, 1777
- Mothé-Diniz, T., Carvano, J., Bus, S., Duffard, R., & Burbine, T. 2008, *Icarus*, **195**, 277
- Mothé-Diniz, T. & Carvano, J. M. 2005, *A&A*, **442**, 727
- Mustard, J. & Hays, J. 1997, *Icarus*, **125**, 145
- Nathues, A., Mottola, S., Kaasalainen, M., & Neukum, G. 2005, *Icarus*, **175**, 452
- Pieters, C. M. & Hiroi, T. 2004, in *Lunar and Planetary Science Conference*, ed. S. Mackwell & E. Stansbery, *Lunar and Planetary Science Conference*, 1720

- Pinto, G. A., Marrocchi, Y., Morbidelli, A., et al. 2021, *ApJLetters*, [917, L25](#)
- Popescu, M., Birlan, M., & Nedelcu, D. A. 2012, *A&A*, [544, A130](#)
- Popescu, M., Licandro, J., Carvano, J. M., et al. 2018, *A&A*, [617, A12](#)
- Reddy, V., Dunn, T. L., Thomas, C. A., Moskovitz, N. A., & Burbine, T. H. 2015, *Mineralogy and Surface Composition of Asteroids* (University of Arizona Press)
- Reddy, V. & Sanchez, J. A. 2016, *NASA Planetary Data System*, EAR–A–10046–3–REDDYMBSPEC–V1.0
- Salisbury, J. W. & Hunt, G. R. 1974, *J. Geophys. Res.*, [79, 4439](#)
- Savitzky, A. & Golay, M. J. E. 1964, *Analytical Chemistry*, [36, 1627](#)
- Schmitt, B., Bollard, P., Albert, D., et al. 2018, SSHADE: "Solid Spectroscopy Hosting Architecture of Databases and Expertise" and its databases., OSUG Data Center. Service/Database Infrastructure.
- Scott, E. R. D. & Krot, A. N. 2014, in *Meteorites and Cosmochemical Processes*, ed. A. M. Davis, Vol. 1, 65–137
- Sunshine, J. M., Connolly, H. C., McCoy, T. J., Bus, S. J., & La Croix, L. M. 2008, *Science*, [320, 514](#)
- Tedesco, E. F., Williams, J. G., Matson, D. L., et al. 1989, *AJ*, [97, 580](#)
- Thomas, C. A. & Binzel, R. P. 2010, *Icarus*, [205, 419](#)
- Vernazza, P., Marsset, M., Beck, P., et al. 2016, *AJ*, [152, 54](#)
- Weisberg, M. K., McCoy, T. J., & Krot, A. N. 2006, *Systematics and evaluation of meteorite classification*, Vol. 19 (University of Arizona Press Tucson)
- Weisberg, M. K., Prinz, M., Clayton, R. N., & Mayeda, T. K. 1997, *Meteoritics and Planetary Science Supplement*, [32, A138](#)
- Xu, S., Binzel, R. P., Burbine, T. H., & Bus, S. J. 1995, *Icarus*, [115, 1](#)

A ASTEROID SPECTRA

Table A.1: References of the asteroid spectra used in this study. Each line refers to one spectrum. If there are several spectra of an individual asteroid, they are denoted using (a), (b), or (c). Two references are given for a single spectrum, they refer to the visible and NIR parts respectively. Columns M22 and DM09 give the taxonomic classifications from [Mahlke et al. \(2022\)](#) and [DeMeo et al. \(2009\)](#) respectively. Barbarian (Bar.) asteroids are indicated following [Devogèle et al. \(2018\)](#). If the asteroid does not appear in the polarimetric database of [Bendjoya et al. \(2022\)](#), it is marked with a dash to indicate that the Barbarian nature is unclear.

Number	Name	M22	DM09	Bar.	Reference
15	Eunomia	K (80%), S (20%)	K	No	DeMeo et al. (2009)
172	Baucis	L (95%)	L	Yes	Devogèle et al. (2018)
221	Eos	K (71%), M (21%), S (8%)	Cb	No	(a) Xu et al. (1995) , Clark et al. (2009) (b) DeMeo et al. (2009)
234	Barbara	L (90%), M (10%) L (71%), S (29%)	L	Yes	(a) Xu et al. (1995) , Gietzen et al. (2012) (b) DeMeo et al. (2009)
236	Honorina	M (87%), P (6%), K (4%)	L	Yes	DeMeo et al. (2009)
387	Aquitania	M (85%), L (15%)	L	Yes	DeMeo et al. (2009)
397	Vienna	L (91%), M (4%) L	L	-	(a) Bus & Binzel (2002b) , Clark et al. (2009) (b) Lazzaro et al. (2007) ; Clark et al. (2009)
402	Chloe	L (88%), M (9%)	L	Yes	DeMeo et al. (2009)
458	Hercynia	M (75%), L (13%), S (13%)	L	Yes	Devogèle et al. (2018)
460	Scania	L	L	-	DeMeo et al. (2009)
579	Sidonia	K (52%), S (47%)	K	-	DeMeo et al. (2009)
599	Luisa	L L M (82%), P (9%), S (7%)	L	Yes	(a) Binzel (2001) , Clark et al. (2009) (b) Xu et al. (1995) , Sunshine et al. (2008) (c) Bus & Binzel (2002b) , Sunshine et al. (2008)
606	Brangane	M (77%), P (21%)	L	Yes	DeMeo et al. (2009)
611	Valeria	M (86%), P (14%)	X	Yes	Devogèle et al. (2018)
653	Berenike	K	K	-	DeMeo et al. (2009)
661	Cloelia	K (88%), M (11%)	K	-	DeMeo et al. (2009)
679	Pax	M (83%), P (6%), S (6%) M (87%), K (8%)	L	Yes	(a) DeMeo et al. (2009) (b) MITHNEOS (Unpublished)
729	Watsonia	M (87%), K (8%), P (5%)	L	Yes	DeMeo et al. (2009)
742	Edisona	K (88%), M (11%)	K	-	DeMeo et al. (2009)
824	Anastasia	L	L	Yes	DeMeo et al. (2009)
980	Anacostia	S (62%), L (20%), M (19%)	S	Yes	Bus & Binzel (2002b) , Sunshine et al. (2008)
1148	Rarahu	K (86%), S (13%)	K	-	DeMeo et al. (2009)
1284	Latvia	P (59%), M (33%), S (7%)	L	Yes	Bus & Binzel (2002b) , Reddy & Sanchez (2016)
1372	Haremari	P (72%), M (27%)	L	Yes	Devogèle et al. (2018)
1545	Therneoe	L	L	-	Bus & Binzel (2002b) , Clark et al. (2009)
1658	Innes	L (60%), S (40%)	Sw	-	DeMeo et al. (2009)
1903	Adzhimush.	K (76%), M (20%)	K	-	DeMeo et al. (2009)
2085	Henan	L (91%), M (6%)	L	Yes	DeMeo et al. (2009)
2354	Lavrov	L L (86%), S (13%)	L	-	(a) Devogèle et al. (2018) (b) DeMeo et al. (2009)
2428	Kamenyar	K (83%), C (17%)	X	-	Vernazza et al. (2016)
2957	Tatsuo	K (51%), M (34%), S (15%)	K	-	DeMeo et al. (2009)
3028	Zhangguoxi	K	Sw	-	DeMeo et al. (2009)
3043	San Diego	L (85%), S (15%)	Sw	-	Lucas et al. (2019)
3066	McFadden	L (92%), S (8%)	Sw	-	Lazzaro et al. (2007) ; Fieber-Beyer et al. (2011)
3734	Waland	L (80%), M (19%)	L	-	DeMeo et al. (2009)
3844	Lujixi	L (90%), S (6%)	L	-	DeMeo et al. (2009)
4737	Kiladze	L	L	-	DeMeo et al. (2009)
4917	Yurilvovia	L (77%), S (12%), M (11%)	L	-	Devogèle et al. (2018)
5840	Raybrown	L (67%), M (27%), S (5%)	L	-	DeMeo et al. (2009)
22771	1999 CU3	L	S	-	DeMeo et al. (2009)
385186	1994 AW1	L	S	-	Binzel et al. (2019)

B REJECTED SPECTRUM